

Real-Time Quadrotor Trajectory Optimization with Time-Triggered Corridor Constraints

Yue Yu^{*} and Kartik Nagpal[†]
The University of Texas at Austin, Austin, TX 78712

Skye Mceowen[‡] and Behçet Açıkmeşe[§]
University of Washington, Seattle, WA 98195

Ufuk Topcu[¶]
The University of Texas at Austin, Austin, TX 78712.

One of the keys to flying quadrotors is to optimize their trajectories within the set of collision-free corridors. These corridors impose nonconvex constraints on the trajectories, making real-time trajectory optimization challenging. We introduce a novel numerical method that approximates the nonconvex corridor constraints with time-triggered convex corridor constraints. This method combines bisection search and repeated infeasibility detection. We further develop a customized C++ implementation of the proposed method, based on a first-order conic optimization method that detects infeasibility and exploits problem structure. We demonstrate the efficiency and effectiveness of the proposed method using numerical simulation on randomly generated problem instances as well as indoor flight experiments with hoop obstacles. Compared with mixed integer programming, the proposed method is about 50–200 times faster.

Nomenclature

Sets

\mathbb{N}	=	the set of positive integers
\mathbb{R}, \mathbb{R}_+	=	the set of real and non-negative real numbers
\mathcal{H}_i	=	the set of feasible position vectors in the i -th corridor
\mathcal{V}	=	the set of feasible velocity vectors
\mathcal{U}_a	=	the set of thrust vectors with pointing direction and magnitude upper bound constraints
\mathcal{U}_b	=	the set of thrust vectors with magnitude lower bound

^{*}Postdoctoral research fellow, Oden Institute of Computational Sciences and Engineering; yueyu@utexas.edu .

[†]Research assistant, Oden Institute of Computational Sciences and Engineering; kartiknagpal@utexas.edu .

[‡]Ph.D. Candidate, The Department of Aeronautics and Astronautics; skye95@uw.edu.

[§]Professor, The Department of Aeronautics and Astronautics; behcet@uw.edu.

[¶]Associate Professor, Oden Institute of Computational Sciences and Engineering; utopcu@utexas.edu

\mathbb{W} = the set of feasible thrust rate

Parameters

m = quadrotor mass

g = acceleration vector caused by gravity

Δ = sampling time period

ω = weighting parameter for thrust rates

c_i, d_i, ρ_i, η_i = center coordinates, direction vector, radius, and length of the i -th cylindrical corridor

ξ = maximum speed

$\underline{\gamma}, \overline{\gamma}, \theta$ = minimum thrust magnitude, maximum thrust magnitude, and maximum tilting angle

δ = maximum thrust rate

\bar{r}_0, \bar{v}_0 = initial position and initial velocity of the quadrotor

$\bar{r}_f, \bar{v}_f, \bar{u}_f$ = final position, final velocity, and final thrust of the quadrotor

Variables

r_k, v_k, u_k = position, velocity, thrust of the quadrotor at time $k\Delta$

τ_i = the length of the trajectory segment for the i -th corridor

t = total length of trajectory

b_{ik} = binary variable, takes value 1 if the quadrotor is in the i -th corridor at time $k\Delta$

I. Introduction

One of the keys to flying quadrotors in a dynamically changing environment is to optimize their trajectories subject to dynamics and collision-avoidance constraints in real-time [1, 2]. Along such a trajectory, the position of the quadrotor needs to stay within a set of *collision-free corridors*. Each corridor is a bounded convex flight space; the union of all these corridors form a nonconvex pathway connecting the quadrotor's current position to its target position [3, 4]; see Fig 1 for a simple illustration. To avoid collisions with obstacles whose positions change rapidly or uncertain, it is critical to update these corridors in real-time. As a result, one needs to optimize trajectories subject to nonconvex corridor constraints in real-time: the faster the optimization, the faster the quadrotor can react to sudden changes of the obstacles.

Since the flight space defined by the union of the corridors is nonconvex, optimizing the trajectories for the quadrotor is computationally challenging. One standard solution approach is *mixed integer programming* [5–7], which first uses binary variables to describe the union of all corridors, then optimizes quadrotor trajectories together with these binary variables [8–11]. However, the worst-case computation time of this approach increases exponentially as the number of binary variables increases. As a result, even with the state-of-the-art solvers—such as GUROBI [12]—real-time quadrotor

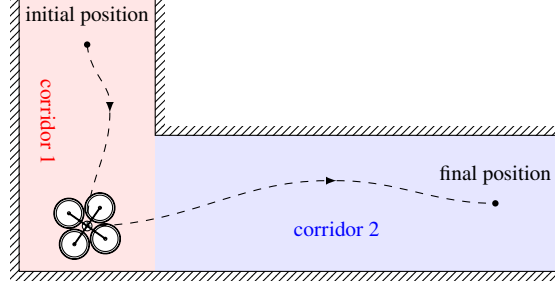


Fig. 1: A quadrotor flight trajectory with corridor constraints.

trajectory optimization via mixed integer programming is still difficult, if at all possible. Alternatively, one can model the corridor constraints as smooth nonconvex constraints and solve the resulting trajectory optimization using the successive convexification method [13]. But this approach suffers from slow computation speed [14], and requires careful parameter tuning to ensure the desired algorithm convergence [15].

Recently, there has been an increasing interest in approximating the nonconvex corridor constraints with time-triggered constraints, where each convex corridor is activated only within one time interval [16–24]. These approximations make the resulting trajectory optimization convex and thus computationally more tractable. However, the existing results have the following limitations. First, they only consider polytopic constraints on trajectory variables, such as elementwise upper and lower bounds on the velocity and acceleration of the quadrotor. These polytopic constraints do not accurately capture the geometric structure of many practical operational constraints—such as the magnitude and pointing direction constraint of the thrust vector [14, 25, 26]—and flight corridors with nonpolytopic boundaries—such as cylindrical or spherical corridors. Second, to our best knowledge, none of the existing methods explicitly test whether the resulting trajectory optimization is feasible. Consequently, the resulting trajectory optimization can be close to infeasible, in which case, a numerical solver will fail to provide a solution; or the trajectory optimization can be far away from being infeasible, which can cause conservative trajectories with unnecessarily long time of flight.

We introduce a novel bisection method that approximates the nonconvex corridor constraints using time-triggered convex corridor constraints, and develop customized implementation of this method that enables real-time quadrotor trajectory optimization subject to general second-order constraints. Our contributions are as follows.

- 1) We theoretically prove that nonconvex corridor constraints are equivalent to time-varying convex corridor constraints, provided that an optimal triggering time for each corridor is known.
- 2) We propose a novel bisection method to estimate the optimal triggering time via repeated infeasibility detection in conic optimization. This method systematically reduces the trajectory length while ensuring that the resulting trajectory optimization is feasible up to a given tolerance. The estimated triggering time reduces a nonconvex trajectory optimization problem to a sequence of convex ones.
- 3) We develop a customized C++ trajectory optimization solver based on the bisection method. This solver

automatically detects infeasibility and exploits the sparsity and geometric structure of trajectory optimization by implementing the proportional-integral projected gradient method (PIPG), an efficient first-order primal-dual conic optimization method.

- 4) We demonstrate the application of the proposed bisection method using numerical simulation and indoor flight experiments. Compared with mixed integer programming, the proposed bisection method and C++ solver shows 50–200 times speedups at the price of an increase in the cost function value by less than 10% .

The implications of our work are threefold. First, our work sets a new benchmark for real-time quadrotor trajectory optimization, which significantly improves the mixed integer programming approach in terms of computation time. Second, our work provides a fresh perspective to deal with nonconvexity in collision avoidance for general autonomous vehicles using bisection search and infeasibility detection. Third, our work demonstrates the potential of PIPG—and in general, first-order optimization methods—in solving nonconvex optimal control problems via not only numerical simulation but also flight experiments.

Notation Given a real number $\alpha \in \mathbb{R}$, we let $\lfloor \alpha \rfloor$ denote the largest integer lower bound of α , and $\lceil \alpha \rceil$ denote the smallest integer upper bound of α . Given a vector r and a matrix M , we let $\|r\|$ denote the ℓ_2 -norm of vector r , $[r]_j$ denote the j -th element of vector r , and $\|M\|$ denote the largest singular value of matrix M . We let 1_n and 0_n denote the n -dimensional vector whose entries are all 1's and all 0's, respectively. We let $0_{m \times n}$ denote the $m \times n$ zero matrix, and I_n denote the $n \times n$ identity matrix. Given a closed convex cone \mathbb{K} , we let \mathbb{K}° denote its polar cone. Given $i, j \in \mathbb{N}$ with $i < j$ and $a_i, a_{i+1}, \dots, a_{j-1}, a_j \in \mathbb{R}^n$, we let $a_{[i,j]} := \begin{bmatrix} a_i^\top & a_{i+1}^\top & \dots & a_{j-1}^\top & a_j^\top \end{bmatrix}^\top$. We say an constrained optimization is *feasible* if its constraints can be satisfied, and *infeasible* otherwise.

II. Three-degree-of-freedom dynamics model for quadrotors

Trajectory optimization for a dynamical system requires a mathematical model that predicts the future state of the system given its current state and input. We introduce a quadrotor dynamics model with three-degrees-of-freedom (3DoF), along with various constraints on the position, velocity, thrust, and thrust rate of the quadrotor. This model lays the foundation of the trajectory optimization problem in the next section.

A. Three degree-of-freedom dynamics

We consider a 3DoF dynamics model for a quadrotor. In particular, at time $s \in \mathbb{R}_+$, we let $r(s) \in \mathbb{R}^3$ and $v(s) \in \mathbb{R}^3$ denote the position and velocity of the center of mass of the quadrotor, and $u(s) \in \mathbb{R}^3$ denote the total thrust force provided by the propellers. Furthermore, we let $m \in \mathbb{R}_+$ and $g = \begin{bmatrix} 0 & 0 & -9.81 \end{bmatrix}^\top$ denote the mass of the quadrotor and the acceleration vector caused by gravity, respectively. The 3DoF continuous-time dynamics model for quadrotor

dynamics is described by the following set of differential equations:

$$\begin{aligned}\frac{d}{ds}r(s) &= v(s), \\ \frac{d}{ds}v(s) &= \frac{1}{m}u(s) + g.\end{aligned}\tag{1}$$

We discretize the above continuous-time differential equation using a first-order-hold scheme. Particularly, we let $\Delta \in \mathbb{R}_+$ denote the discretization step size. Let

$$r_k := r(k\Delta), \quad v_k := v(k\Delta), \quad u_k := u(k\Delta),\tag{2}$$

for all $k \in \mathbb{N}$. We apply a piecewise linear input thrust such within each $\Delta \in \mathbb{R}_+$ time interval, *i.e.*,

$$u(s) = \left(k + 1 - \frac{s}{\Delta}\right)u_k + \left(\frac{s}{\Delta} - k\right)u_{k+1},\tag{3}$$

for all $k\Delta \leq s \leq (k+1)\Delta$. Under this assumption, the equations in (1) are equivalent to the following:

$$\begin{aligned}r_{k+1} &= r_k + \Delta v_k + \frac{\Delta^2}{3m} \left(u_k + \frac{1}{2}u_{k+1}\right) + \frac{\Delta^2}{2}g, \\ v_{k+1} &= v_k + \frac{\Delta}{2m}(u_k + u_{k+1}) + \Delta g,\end{aligned}\tag{4}$$

for all $k \in \mathbb{N}$.

B. Position, velocity, and thrust constraints

The position, velocity, and thrust vector of the quadrotor are subject to the following constraints.

1. Position

The quadrotor's position is constrained within the union of a set of three-dimensional cylinders, or *corridors*. We let $l \in \mathbb{N}$ denote the total number of corridors. For the i -th corridor, we let $c_i \in \mathbb{R}^3$ denote its center, $d_i \in \mathbb{R}^3$ with $\|d_i\| = 1$ denote its direction vector, $\eta_i \in \mathbb{R}_+$ and $\rho_i \in \mathbb{R}_+$ denote its half-length and radius, respectively. See Fig. 2 for an illustration. We define the i -th corridor as follows:

$$\mathbb{H}_i := \{c_i + r \in \mathbb{R}^3 \mid \|r - \langle d_i, r \rangle d_i\| \leq \rho_i, |\langle d_i, r \rangle| \leq \eta_i\}.\tag{5}$$

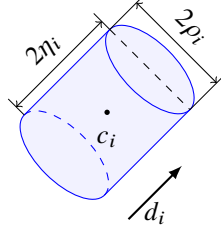


Fig. 2: A illustration of the set \mathbb{H}_i in (5).

2. Velocity

The quadrotor's speed is upper bounded by $\xi \in \mathbb{R}_+$. The set of feasible velocity vectors is as follows:

$$\mathbb{V} := \{v \in \mathbb{R}^3 \mid \|v\| \leq \xi\}. \quad (6)$$

3. Thrust

The thrust vectors of the quadrotor are subject to the following two different set of constraints: magnitude constraints and direction constraints.

Magnitude constraints The Euclidean norm of the thrust vector is upper bounded by $\bar{\gamma} \in \mathbb{R}_+$, and the thrust along the direction opposite to the gravity is lower bounded by $\underline{\gamma} \in \mathbb{R}_+$.

Direction constraints The direction of the thrust vector is constrained as follows: the angle between the thrust direction and the the direction opposite to the gravity is no more than a fixed angle $\theta \in [0, \frac{\pi}{2}]$.

The above constraints on the thrust magnitude and direction ensure that the on-board motors can provide the thrust needed, and the tilting angle of the quadrotor is upper bounded. See Fig. 3 for an illustration of the tilting angle. By

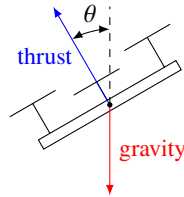


Fig. 3: Tilting angle θ of the quadrotor.

combining the aforementioned constraints, we define the set of feasible thrust vectors as the intersection of the following two sets:

$$\mathbb{U}_a := \{u \in \mathbb{R}^3 \mid \|u\| \leq \bar{\gamma}, \cos \theta \|u\| \leq [u]_3\}, \quad (7a)$$

$$\mathbb{U}_b := \{u \in \mathbb{R}^3 \mid [u]_3 \geq \underline{\gamma}\}. \quad (7b)$$

4. Thrust rate

The difference between two consecutive thrust vectors, termed a *thrust rate vector*, is subject to an upper bound of $\delta \in \mathbb{R}_+$ on its Euclidean norm. The set of all feasible thrust rate vectors is as follows:

$$\mathbb{W} := \{w \in \mathbb{R}^3 \mid \|w\| \leq \delta\}. \quad (8)$$

The constraints in (8) prevents large changes in the thrust vector within a Δ -seconds time interval, hence ensuring the smoothness of the thrust trajectory.

III. Trajectory optimization with time-triggered constraints

We will introduce the quadrotor trajectory optimization with time-triggered corridor constraints. To this end, we will first consider the trajectory optimization with nonconvex corridor constraints, then propose an approximate problem that replaces these nonconvex corridor constraints with convex ones.

A. Trajectory optimization with nonconvex corridor constraints

We will introduce a trajectory optimization problem subject to nonconvex corridor constraints. In this problem, we use the quadrotor dynamics in (4). We let $t \in \mathbb{N}$ denote the total length of the trajectory. We let $\bar{r}_0, \bar{v}_0 \in \mathbb{R}^3$ denote the known initial position and initial velocity of the quadrotor, respectively. Similarly, we let $\bar{r}_f, \bar{v}_f, \bar{u}_f \in \mathbb{R}^3$ denote the known final position, final velocity, and final thrust of the quadrotor, respectively. We will use the set \mathbb{V} , \mathbb{U} and \mathbb{W} defined in (6), (7), and (8), respectively. We let $\{\mathbb{H}_1, \mathbb{H}_2, \dots, \mathbb{H}_l\}$ denote a sequence of corridors, where \mathbb{H}_i is defined by (5) for all $i \in [1, l]$.

We now introduce the following quadrotor trajectory optimization with nonconvex state constraints, where $\omega \in \mathbb{R}_+$ is a weight scalar for the cost for the thrust rates: by changing the value of ω , one can obtain different trade-offs between cost for the thrust and the thrust rates.

Trajectory optimization with nonconvex corridor constraints

$$\begin{aligned}
& \underset{u_{[0,t]}}{\text{minimize}} \quad \frac{1}{2} \sum_{k=0}^t \|u_k\|^2 + \frac{\omega}{2} \sum_{k=0}^{t-1} \|u_{k+1} - u_k\|^2 \\
& \text{subject to} \\
& r_{k+1} = r_k + \Delta v_k + \frac{\Delta^2}{3m} (u_k + \frac{1}{2} u_{k+1}) + \frac{\Delta^2}{2} g, \\
& v_{k+1} = v_k + \frac{\Delta}{2m} (u_k + u_{k+1}) + \Delta g, \quad \forall k \in [0, t-1], \\
& u_{k+1} - u_k \in \mathbb{W}, \quad \forall k \in [0, t-1], \\
& u_k \in \mathbb{U}_a \cap \mathbb{U}_b, \quad v_k \in \mathbb{V}, \quad r_k \in \bigcup_{i=1}^l \mathbb{H}_i, \quad \forall k \in [0, t], \\
& r_0 = \bar{r}_0, \quad v_0 = \bar{v}_0, \quad r_t = \bar{r}_f, \quad v_t = \bar{v}_f, \quad u_t = \bar{u}_f.
\end{aligned} \tag{9}$$

Optimization (9) is equivalent to a mixed integer optimization problem. To see this equivalence, notice that optimization (9) contains the following constraints:

$$r_k \in \bigcup_{i=1}^l \mathbb{H}_i, \quad \forall k \in [0, t]. \tag{10}$$

The constraints in (10) are equivalent to the following set of constraints with binary variables:

$$\|(r_k - c_i) - \langle d_i, r_k - c_i \rangle\| \leq b_{ik} \rho_i + \mu(1 - b_{ik}), \tag{11a}$$

$$|\langle d_i, r_k - c_i \rangle| \leq b_{ik} \eta_i + \mu(1 - b_{ik}), \tag{11b}$$

$$b_{ik} \in \{0, 1\}, \quad \sum_{i=1}^l b_{ik} \geq 1, \quad \forall k \in [0, t], i \in [1, l], \tag{11c}$$

where $\mu \in \mathbb{R}_+$ denotes a very large positive scalar. Indeed, if $b_{ik} = 0$, then the constraints in (11a) and (11b) become redundant, since μ is very large. On the other hand, if $b_{ik} = 1$, then the constraints in (11a) and (11b) imply that $r_k \in \mathbb{H}_i$. Finally, the constraints in (11c) ensure that there exists $i \in [1, l]$ such that $b_{ik} = 1$, hence $r_k \in \mathbb{H}_i$ for some $i \in [1, l]$. Therefore, the constraints in (10) and (11) are equivalent.

Since optimization (9) is equivalent to a mixed-integer optimization, the computation time for solving optimization (9) increases exponentially as the number of integer variables—in this case, jointly determined by the trajectory length τ and number of corridors l —increases. Consequently, a real-time solution method is only possible if the values of τ and n are both sufficiently small.

B. Trajectory optimization with time-triggered corridor constraints

We will show that optimization (9) takes a simpler form if we know *a priori* the sequence of corridors that the optimal trajectory traverses. To this end, we start with the following assumption on the ordering of corridor sequence $\{\mathbb{H}_1, \mathbb{H}_2, \dots, \mathbb{H}_l\}$.

Assumption 1. Suppose optimization (9) is feasible. Let $u_{[0,t]}$ be an optimal thrust trajectory for optimization (9), and $r_{[0,t]}$ and $u_{[0,t]}$ satisfy the constraints in optimization (9). There exists $\tau_1, \tau_2, \dots, \tau_l \in \mathbb{R}_+$ such that $t = \sum_{j=1}^l \tau_j$ and $r_k \in \mathbb{H}_i$ for all $k \in [\sum_{j=1}^{i-1} \tau_j, \sum_{j=1}^i \tau_j]$ and $i \in [1, l]$, where $\sum_{j=1}^0 \tau_j := 0$.

For Assumption 1 to hold, we need to know *a priori* the ordered sequence of corridors that order in which the optimal trajectory traverses. Many corridor generating algorithms, such as convex lifting, can provide such an ordered sequence of corridors; see [3, 4] for some recent examples.

Assumption 1 also implies that no corridor appeared more than once along the optimal corridor path. Since reentering the same corridor twice will increase the value of the objective function in optimization (9), such an implication always holds in practice.

Under Assumption 1, it is tempting to replace the nonconvex corridor constraints in (10) with time-varying constraints. After this replacement, optimization (9) becomes the following optimization in (12).

Trajectory optimization with time-triggered corridor constraints

$$\begin{aligned}
& \underset{u_{[0,t]}}{\text{minimize}} \quad \frac{1}{2} \sum_{k=0}^t \|u_k\|^2 + \frac{\omega}{2} \sum_{k=0}^{t-1} \|u_{k+1} - u_k\|^2 \\
& \text{subject to} \\
& r_{k+1} = r_k + \Delta v_k + \frac{\Delta^2}{3m} (u_k + \frac{1}{2} u_{k+1}) + \frac{\Delta^2}{2} g, \\
& v_{k+1} = v_k + \frac{\Delta}{2m} (u_k + u_{k+1}) + \Delta g, \quad \forall k \in [0, t-1], \\
& u_{k+1} - u_k \in \mathbb{W}, \quad \forall k \in [0, t-1], \\
& u_k \in \mathbb{U}_a \cap \mathbb{U}_b, \quad v_k \in \mathbb{V}, \quad \forall k \in [0, t], \\
& r_k \in \mathbb{H}_i, \quad \forall k \in [\sum_{j=1}^{i-1} \tau_j, \sum_{j=1}^i \tau_j], \quad i \in [1, l], \\
& r_0 = \bar{r}_0, \quad v_0 = \bar{v}_0, \quad r_t = \bar{r}_f, \quad v_t = \bar{v}_f, \quad u_t = \bar{u}_f.
\end{aligned} \tag{12}$$

The following proposition shows that, under Assumption 1, solving optimization (12) is equivalent to solving optimization (9).

Proposition 1. Suppose that Assumption 1 holds. If $u_{[0,t]}^*$ is an optimal thrust trajectory for optimization (12), then $u_{[0,t]}^*$ is an optimal thrust trajectory for optimization (9).

Proof. Since Assumption (1) holds, optimization (9) has at least one optimal solution, and so does optimization (12).

Let $u_{[0,t]}^*$ be an optimal solution for optimization (12), $u_{[0,t]}$ be an optimal solution for optimization (9), $\phi(u_{[0,t]}) = \frac{1}{2} \sum_{k=0}^t \|u_k\|^2 + \frac{\omega}{2} \sum_{k=0}^{t-1} \|u_{k+1} - u_k\|^2$, and $\phi(u_{[0,t]}^*) = \frac{1}{2} \sum_{k=0}^t \|u_k^*\|^2 + \frac{\omega}{2} \sum_{k=0}^{t-1} \|u_{k+1}^* - u_k^*\|^2$.

First, since trajectory $u_{[0,t]}$ also satisfies the constraints in (12) and $u_{[0,t]}^*$ is optimal for optimization (12), we must have $\phi(u_{[0,t]}^*) \leq \phi(u_{[0,t]})$.

Second, Assumption 1 implies that $u_{[0,t]}^*$ also satisfies the constraints in optimization (9). Combining this fact with the assumption that $u_{[0,t]}$ is optimal for optimization (9), we conclude that $\phi(u_{[0,t]}) \leq \phi(u_{[0,t]}^*)$.

Therefore we conclude that $u_{[0,t]}^*$ satisfies the constraints in optimization (9) and $\phi(u_{[0,t]}^*) = \phi(u_{[0,t]})$. Hence $u_{[0,t]}^*$ is also optimal for optimization (9). \square

Proposition 1 provides valuable insights in solving optimization (9): rather than the value of the $(t+1)l$ binary variables in (11), we only need to determine the value of l integers that determines the triggering time, given by $\tau_1, \tau_2, \dots, \tau_l$, in optimization (12). Although computing the exact value of this sequence is as difficult as solving optimization (9) itself, one can compute a good approximation very efficiently, as we will show next.

C. Computing the triggering time via bisection method

In this section, we introduce a numerical algorithm for optimization (12) using an approximate triggering time sequence $\tau_{[1,l]}$. To this end, we make the following assumption about optimization (12).

Assumption 2. *There exists $\underline{\tau}_1, \underline{\tau}_2, \dots, \underline{\tau}_l$ and $\bar{\tau}_1, \bar{\tau}_2, \dots, \bar{\tau}_l$ with $\underline{\tau}_j \leq \bar{\tau}_j$ for all $j = 1, 2, \dots, l$, such that 1) optimization (12) is feasible if $\tau_{[1,l]} = \bar{\tau}_{[0,l]}$ and $t = \sum_{j=1}^l \bar{\tau}_j$, and 2) optimization (12) is infeasible if $\tau_{[1,l]} = \underline{\tau}_{[0,l]}$ and $t = \sum_{j=1}^l \underline{\tau}_j$.*

Remark 1. *Assumption 1 implies that optimization (12) is feasible if we allocate an sufficient amount of time for each corridor, and infeasible otherwise. Using the length of each corridor and an upper and lower bounds on the average speed of the quadrotor, we can obtain an interval estimate for each corridor.*

Given lower and upper bound sequences that satisfy Assumption 1, we introduce a heuristic method, summarized in Algorithm 1. The idea is to first use a bisection search method to tighten the interval bounds for each corridor, one at a time. Then using these tightened upper bounds to solve optimization (12).

We note that the upper bound sequence $\bar{\tau}_{[0,l]}$ computed by the for-loop between line 1 and line 11 in Algorithm 1 is not necessarily the same sequence in Assumption 1. Consequently the instance of optimization (12) solved in line 12 is merely an *approximation* of optimization (9). However, such an approximation has the following attractive properties. First a feasible solution is guaranteed to exist by construction, and each convex corridor constraint is active within the corresponding time interval. Second, up to the accuracy tolerance ϵ , each element of the upper bound sequence is reduced greedily until optimization (12) becomes infeasible, which reduces the conservativeness of the initial estimates.

Algorithm 1 Trajectory optimization with time-triggered corridor constraints

Input: Two time sequence $\bar{\tau}_{[1,l]}$ and $\underline{\tau}_{[1,l]}$ that satisfy Assumption 2, positive accuracy tolerance ϵ .

```
1: for  $i = 1, 2, \dots, l$  do
2:   while  $\bar{\tau}_i - \underline{\tau}_i > \epsilon$  do
3:      $\hat{\tau}_j = \begin{cases} \lfloor \frac{1}{2}(\bar{\tau}_i + \underline{\tau}_i) \rfloor, & \text{if } j = i. \\ \bar{\tau}_j, & \text{otherwise.} \end{cases}$ 
4:     Let  $t = \sum_{j=1}^l \hat{\tau}_j$  and  $\tau_{[1,l]} = \hat{\tau}_{[1,l]}$  in optimization (12).
5:     if optimization (12) is infeasible then
6:        $\underline{\tau}_i \leftarrow \hat{\tau}_i$ 
7:     else
8:        $\bar{\tau}_i \leftarrow \hat{\tau}_i$ 
9:     end if
10:   end while
11: end for
12: Let  $\tau_{[1,l]} = \bar{\tau}_{[1,l]}$  and  $t = \sum_{j=1}^l \bar{\tau}_j$  in optimization (12), then solve for the optimal trajectory  $u_{[0,\tau]}^*$ .
Output:  $u_{[0,t]}^*$ 
```

IV. Real-time conic optimization with infeasibility detection

The key step in Algorithm 1 is to solve optimization (12) if it is feasible, and prove that it is infeasible otherwise. Such a problem is also known as *infeasibility detection* in constrained optimization. In this section we introduce an infeasibility detection method customized for optimization (12). This method is based on the proportional-integral projected gradient method (PIPG), a primal-dual conic optimization method [27–30].

A. Reformulating a trajectory optimization as a conic optimization

Conic optimization is the minimization of a convex objective function subject to conic constraints. In the following, we will reformulate the trajectory optimization problem in (12) as a special case of conic optimization. To this end, we need to rewrite the objective function and constraints in optimization (12) in a more compact form as follows. First, we introduce the following trajectory variable:

$$x := \begin{bmatrix} r_{[0,t]}^\top & v_{[0,t]}^\top & u_{[0,t]}^\top & w_{[0,t-1]}^\top \end{bmatrix}^\top. \quad (13)$$

where $w_k := u_{k+1} - u_k$ for all $k \in [0, t-1]$. With this variable, we can rewrite the quadratic objective function in optimization (12) as follows:

$$\frac{1}{2} x^\top \underbrace{\text{diag} \left(\begin{bmatrix} 0_{6(t+1)}^\top & 1_{3(t+1)}^\top & \omega 1_{3t}^\top \end{bmatrix} \right)}_P x. \quad (14)$$

Second, we define the following submatrices:

$$\begin{aligned}
H_{11} &= \begin{bmatrix} 0_{3t \times 3} & I_{3t} \end{bmatrix} - \begin{bmatrix} I_{3t} & 0_{3t \times 3} \end{bmatrix}, \\
H_{12} &= -\Delta \begin{bmatrix} I_{3t} & 0_{3t \times 3} \end{bmatrix}, \quad H_{14} = 0_{3t \times 3t}, \\
H_{13} &= -\frac{\Delta^2}{3m} \begin{bmatrix} 0_{3t \times 3} & I_{3t} \end{bmatrix} - \frac{\Delta^2}{6m} \begin{bmatrix} I_{3t} & 0_{3t \times 3} \end{bmatrix}, \\
H_{21} &= 0_{3t \times 3(t+1)}, \quad H_{22} = H_{11}, \quad H_{24} = 0_{3t \times 3t}, \\
H_{23} &= -\frac{\Delta}{2m} \begin{bmatrix} 0_{3t \times 3} & I_{3t} \end{bmatrix} - \frac{\Delta}{2m} \begin{bmatrix} I_{3t} & 0_{3t \times 3} \end{bmatrix}, \\
H_{31} &= H_{32} = 0_{3t \times 3(t+1)}, \quad H_{33} = H_{11}, \\
H_{34} &= I_{3t}, \quad H_{41} = H_{42} = 0_{(t+1) \times 3(t+1)}, \\
H_{43} &= I_{t+1} \otimes \begin{bmatrix} 0 & 0 & 1 \end{bmatrix}, \quad H_{44} = 0_{(t+1) \times 3t}.
\end{aligned} \tag{15}$$

With the definition in (13) and (15), we can rewrite the linear equality and inequality constraints in optimization (12)–which include the linear dynamics constraints and the linear lower bound constraints on the thrust vectors—equivalently as follows:

$$\underbrace{\begin{bmatrix} H_{11} & H_{12} & H_{13} & H_{14} \\ H_{21} & H_{22} & H_{23} & H_{24} \\ H_{31} & H_{32} & H_{33} & H_{34} \\ H_{41} & H_{42} & H_{43} & H_{44} \end{bmatrix}}_H x - \underbrace{\begin{bmatrix} 0_{9t} \\ \underline{\gamma} 1_{t+1} \end{bmatrix}}_b \in \underbrace{\{0_{9t}\} \times \mathbb{R}_+^{t+1}}_{\mathbb{K}}, \tag{16}$$

Note that $\underline{\gamma} \in \mathbb{R}_+$ is the thrust lower bound introduced in (7b).

Third, we define the following closed convex set

$$\mathbb{D}_i = \mathbb{H}_i \times \mathbb{V} \times \mathbb{U}_a \times \mathbb{W}, \tag{17}$$

for all $i = 1, 2, \dots, l$, where set \mathbb{H}_i , \mathbb{V} , \mathbb{W} are given in (5), (6), (8), respectively; set \mathbb{U}_a is given by (7a).

Notice the only difference between set $\mathbb{U}_a \cap \mathbb{U}_b$ and set \mathbb{U}_a is that the latter does not include the linear lower bound constraint in \mathbb{U}_b ; this constraint is already included in the last $t + 1$ linear inequality constraints in (16). With these sets, we can compactly rewrite the second-order-cone constraints in optimization (12)—which include those for position,

velocity, thrust, and thrust rate vectors—as follows:

$$x \in \underbrace{(\mathbb{D}_1)^{\tau_1} \times (\mathbb{D}_2)^{\tau_2} \times \cdots \times (\mathbb{D}_l)^{\tau_l}}_{\mathbb{D}}, \quad (18)$$

where $(\mathbb{D}_i)^{\tau_i}$ is the Cartesian product of τ_i copies of set \mathbb{D}_i .

With the above definition, we can now rewrite optimization (12) equivalently as optimization (19), where matrix P is given in (14); matrix H , vector b , cone \mathbb{K} are given in (16); set \mathbb{D} is given in (18).

Conic optimization

$$\begin{aligned} & \underset{x}{\text{minimize}} && \frac{1}{2}x^\top Px \\ & \text{subject to} && Hx - b \in \mathbb{K}, \quad x \in \mathbb{D}. \end{aligned} \quad (19)$$

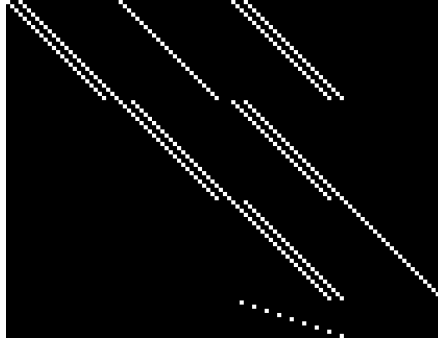


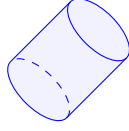
Fig. 4: The sparsity pattern of matrix H in (16). Each zero and nonzero entry corresponds to a black and white pixel, respectively.

Optimization (19) has two salient features: the sparsity pattern of matrix P and H , and the geometric structure of set \mathbb{D} . First, matrix P is diagonal, and matrix H has many zero elements; see Fig. 4 for an illustration. The presence of these zero elements is because the dynamics constraints in (4) only apply to variables corresponding to adjacent time steps. Second, set \mathbb{D} is a Cartesian product of many simple sets, such as cylinder, ball, or the intersection of an icecream cone and a ball. See Fig. 5 for an illustration.

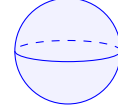
B. Proportional-integral projected gradient method

To exploit the salient features of optimization (19), we propose to use the proportional-integral projected gradient method (PIPG). PIPG is a state-of-the-art first-order primal-dual optimization method that combines the idea of projected gradient method and proportional-integral feedback of constraint violation; such a combination was first introduced in distributed optimization [31, 32] and later extended to optimal control problems [27–30].

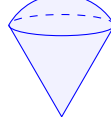
Algorithm 2 is the pseudocode implementation of PIPG with extrapolation [30], where $\Pi_{\mathbb{D}}$ and $\Pi_{\mathbb{K}}$ denote the



(a) Cylinder.



(b) Ball.



(c) The intersection of an icecream cone and a ball.

Fig. 5: An illustration of the geometric structure of the simple sets that constitute the set \mathbb{D} in (18).

Euclidean projection map onto set \mathbb{D} and the polar cone of cone \mathbb{K} , respectively; these projection maps will be discussed in details later. The if-clause between line 9 and line 13 determines whether optimization (19) is infeasible by monitoring the difference between two consecutive iterates [30].

Algorithm 2 PIPG for convex trajectory optimization

Input: Parameters in optimization (19), number of iterations j_{\max} , step sizes α, β, λ , feasibility tolerance ϵ

1: Randomly initialize $x, \bar{x} \in \mathbb{R}^{12r+9}$, $y, \bar{y} \in \mathbb{R}^{10r+1}$.

2: **for** $j = 1, 2, \dots, j_{\max}$ **do**

3: $y^- \leftarrow y$

4: $x \leftarrow \Pi_{\mathbb{D}}[\bar{x} - \alpha(P\bar{x} + H^T\bar{y})]$

5: $y \leftarrow \Pi_{\mathbb{K}^\circ}[\bar{y} + \beta(H(2x - \bar{x}) - g)]$

6: $\bar{x} \leftarrow (1 - \lambda)\bar{x} + \lambda x$

7: $\bar{y} \leftarrow (1 - \lambda)\bar{y} + \lambda y$

8: **end for**

9: **if** $\frac{\|y - y^-\|}{\beta\lambda\|x\|} \leq \epsilon$ **then**

10: **return** x

11: **else**

12: **return** "Infeasible"

13: **end if**

Output: x or "Infeasible".

Compared with other numerical methods for optimization (19), PIPG has the following advantages. First, PIPG does not compute the inverse of any matrices or solve any linear equation systems, making it suitable for real-time implementation with light digital footprints [29]. Second, compared with other first-order methods, PIPG achieves the fastest convergence rates in terms of both the primal-dual gap and constraint violation [28]. Third, PIPG automatically generates proof of infeasibility if possible [29, 30]. When solving optimal control problems, PIPG is much faster than many state-of-the-art optimization solvers in numerical experiments [30].

C. Implementation

In order to implement Algorithm 2, we need to determine several algorithm parameters, and efficiently compute the projections in line 4 and line 5 of Algorithm 2. We will discuss these implementation details in the following.

1. Parameter selection

Step sizes The iterates of PIPG converge if parameter α and β satisfy the following constraint, which is a special case of those in [30, Rem. 1]:

$$0 < \alpha = \beta < \frac{2}{\sqrt{\|P\|^2 + 4\|H\|^2}}. \quad (20)$$

By using the definition of matrix P in (14), one can verify that $\|P\| = \max\{1, \omega\}$, where ω is the weighting parameter in the objective function in optimization (12). As for the value of $\|H\|^2$, we compute an approximate of it using the *power iteration algorithm* [33], summarized in Algorithm 3.

Algorithm 3 The power iteration method [33]

Input: Matrix $H \in \mathbb{R}^{(10t+1) \times (12t+9)}$, accuracy tolerance ϵ .

- 1: Randomly initialize $x \in \mathbb{R}^{12t+9}$; let $\sigma = \|x\|$, $\sigma^- = \epsilon + \sigma$.
- 2: **while** $|\sigma - \sigma^-| \geq \epsilon$ **do**
- 3: $\sigma^- \leftarrow \sigma$
- 4: $y \leftarrow \frac{1}{\sigma} Hx$
- 5: $x \leftarrow H^\top y$
- 6: $\sigma \leftarrow \|x\|$
- 7: **end while**

Output: σ .

As for parameter λ —which denotes the step length of extrapolation in PIPG [30]—numerical experiments shows that values between 1.6 and 1.9 leads to the best convergence performance in practice [30]. In our implementation, we let $\lambda = 1.9$.

Maximum number of iteration and feasibility tolerance As a first order method, PIPG tends to converge within hundreds of iterations. In the implementation of Algorithm 2, we set $j_{\max} = 10^4$ and $\epsilon = 10^{-3}$.

2. Computing the projections

We now provide explicit formulas for computing the projections onto the closed convex sets that constitute the set \mathbb{D} in (18); see Fig. 5 for an illustration. For projection formulas of other closed convex sets, such as the cone \mathbb{K} in (16), we refer the interested readers to [34, Chp. 29].

Cylinder Given a position vector $r \in \mathbb{R}^3$, the projection of r onto the set \mathbb{H}_i in (5) is given as follows [34, Exe. 29.1]:

$$\Pi_{\mathbb{H}_i}[r] = \max(-\eta_i, \min(\eta_i, r_a)) + \frac{\rho_i}{\max(\|r_b\|, \rho_i)} r_b, \quad (21)$$

where

$$r_a = \langle d_i, r \rangle d_i, \quad r_b = r - \langle d_i, r \rangle d_i. \quad (22)$$

Ball Given a velocity vector $v \in \mathbb{R}^3$, the projection of v onto the set \mathbb{V} in (6) is given as follows [34, Prop. 29.10]:

$$\Pi_{\mathbb{V}}[v] = \frac{\xi}{\max(\xi, \|v\|)} v. \quad (23)$$

The projection onto set (8) is similar.

The intersection of a ball and an icecream cone Computing a projection onto the intersection of a icecream cone and a ball is the same as first computing a projection onto the icecream cone then computing a projection onto the ball [35, Thm. 7.1]. In particular, give a thrust vector $u \in \mathbb{R}^3$, the projection of u onto the set \mathbb{U}_a in (7a) is given by

$$\Pi_{\mathbb{U}_a}[u] = \frac{\bar{\gamma}}{\max(\bar{\gamma}, \|u_a\|)} u_a, \quad (24)$$

where

$$u_a = \begin{cases} u, & \text{if } \cos \lambda \|u\| \leq [u]_3, \\ 0, & \text{if } \sin \lambda \|u\| \leq -[u]_3, \\ \langle u, u_b \rangle u_b, & \text{otherwise,} \end{cases} \quad (25)$$

and

$$u_b = \begin{bmatrix} 0 \\ 0 \\ \cos \lambda \end{bmatrix} + \frac{\sin \lambda}{\sqrt{([u]_1)^2 + ([u]_2)^2}} \begin{bmatrix} [u]_1 \\ [u]_2 \\ 0 \end{bmatrix}. \quad (26)$$

The formula in (24) is similar to that in (23). The formula in (25) is a special case of the projection formula of an icecream cone [34, Exe. 29.12].

V. Numerical simulation and indoor flight experiments

We demonstrate the efficiency of Algorithm 2 by comparing its computation time against the state-of-the-art optimization solvers, and demonstrate the effectiveness of the trajectories computed by Algorithm 2 using indoor flight experiments via a custom quadrotor.

A. Numerical simulation with randomly generated corridors

We first evaluate the efficiency of the algorithms developed in Section III and Section IV using instances of optimization (9) with randomly generated corridors as follows. First, we let

$$\bar{r}_0 = \bar{v}_0 = \bar{v}_f = \begin{bmatrix} 0 & 0 & 0 \end{bmatrix}^\top, \quad \bar{u}_f = -g. \quad (27)$$

Second, we set the scalar parameters in optimization (9) using the values listed in Table 1. Third, we generate 100 random sequences of corridors, see Fig. 6 for an illustration of the center lines of these corridor sequences. Each sequence contains 7 corridors. Each corridor starts at the origin and is uniquely characterized by four scalar parameters: radius, length, and two angles that defines its direction in a spherical coordinates—azimuthal angle and elevation angle. Each scalar parameter is sampled from a uniform distribution over an interval, see Table 2 for the interval bounds of these parameters. Finally, we vary the number of corridors traversed by the trajectory by setting the final position \bar{r}_f to be the end point of different corridors in each sequence.

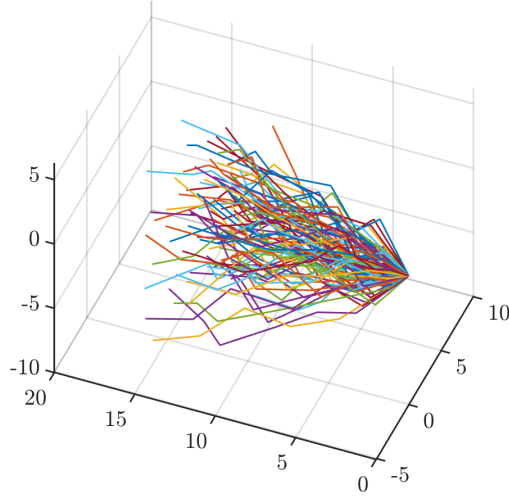


Fig. 6: The center lines of the 100 random sequences of corridors.

Table 1: The parameter values in optimization (9) (all units are omitted for simplicity)

m	Δ	ω	ξ	γ	$\bar{\gamma}$	θ	δ
0.35	0.20	1.00	3.00	2.00	5.00	$\frac{\pi}{4}$	3.00

Table 2: The interval bounds of the corridor parameters.

parameter	interval
radius	$[0.10, 0.50]$
length	$[1.00, 4.00]$
azimuthal angle	$[\frac{\pi}{4}, \frac{3\pi}{4}]$
elevation angle	$[-\frac{\pi}{4}, \frac{\pi}{4}]$

We demonstrate the performance of Algorithm 1 using the aforementioned random instances of optimization (9), where we use Algorithm 2 for infeasibility detection and optimizing a trajectory with time-varying corridor constraints. We implement the combination of Algorithm 1 and Algorithm 2 in C++; see <https://github.com/Kartik->

Nagpal/PIPG-Cpp for details. We choose the values of time sequence $\bar{\tau}_{[1,l]}$ and $\underline{\tau}_{[1,l]}$ in Algorithm 1 using the length of each corridor and the quadrotor’s maximum speed, given by ξ ; and a coarse estimates of its minimum speed, given by $\xi/2$.

Fig. 7 shows the computation time and solution quality of Algorithm 1 combined with Algorithm 2, and compares them against the performance of various combinations of Algorithm 1, mixed integer programming (MIP), off-the-shelf parser YALMIP [36], commercial conic optimization solver GUROBI [12], and open-source conic optimization solver ECOS [37]. All numerical experiments are executed on a desktop computer equipped with the AMD Ryzen 9 5900X 12 Core Processor. Overall the combination of Algorithm 1 and Algorithm 2 is about 50–200 times faster than the MIP approach as well as the combination of Algorithm 1 and off-the-shelf solvers, at the price of at most a 10% increase in the cost function value.

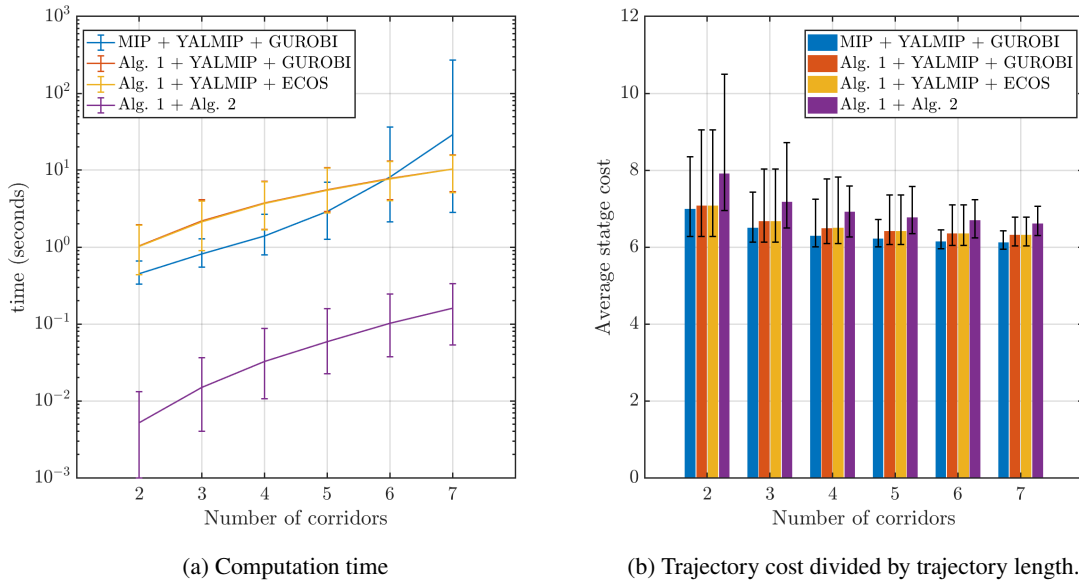


Fig. 7: The comparison of the computation time and the average state cost—which equals the objective function in optimization (9) divided by trajectory length t —of the trajectories computed by different solvers for optimization (9), averaged over 100 randomly generated scenarios. The error bar shows the maximum and minimum value.

B. Indoor flight experiments with hoop obstacles

We demonstrate the application of Algorithm 1 and Algorithm 2 using the quadrotor platform in the Autonomous Control Laboratory (see <https://depts.washington.edu/uwac1/>). This platform contains a custom-made quadrotor equipped with a 2200-milliAmp-hour lithium-polymer battery; accelerometers and gyroscopes that measure the acceleration and the angular velocity, respectively, at a 100-1000 Hz rate; a 500 MHz dual-core Intel Edison and a 1.7 GHz quad-core Intel Joule processor; and an IEEE 802.11n compliant WiFi communication link. See Fig. 8 for an illustration. The platform also include an 4 meters by 7 meters by 3 meters indoor flight space, equipped with an

OptiTrack motion capture system that can measure the attitude and position of a quadrotor at 50-150 Hz rate.

We conduct the quadrotor flight experiments using the trajectories computed by Algorithm 1 and Algorithm 2 as reference guidance. We also use hoop obstacles to mark out the boundary of each flight corridor. Fig. 10 shows the reference trajectories and experiment trajectories in three different corridor scenarios*. These experiments demonstrate how to use the proposed approach in actual flight experiments in cluttered environments.

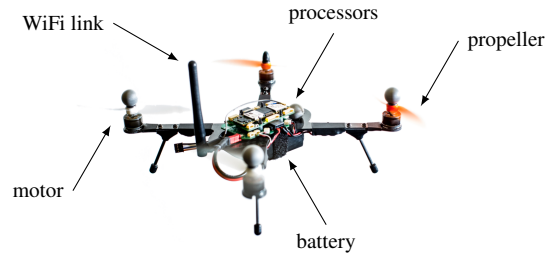


Fig. 8: The custom quadrotor in the Autonomous Control Laboratory.

VI. Conclusion

We introduce a novel bisection method that approximates the nonconvex corridor constraints using time-triggered convex corridor constraints, and develop customized implementation of this method that enables real-time trajectory optimization subject to second-order cone constraints. Our results provide a novel benchmark solution approach for trajectory optimization, which is about 50–200 times faster than mixed integer programming in numerical experiments. Future direction includes onboard implementation and extensions to trajectory optimization with nonlinear dynamics model, such as six-degree-of-freedom rigid body dynamics for space vehicles [38].

References

- [1] Elmokadem, T., and Savkin, A. V., “Towards Fully Autonomous UAVs: A Survey,” *Sensors*, Vol. 21, No. 18, 2021, p. 6223.

*To ensure flight safety, we use a reduced hoop radius (about 20% of the actual size) when computing the flight trajectories.

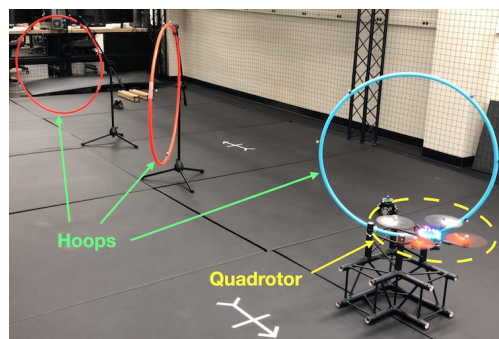


Fig. 9: The indoor flight environment with hoop obstacles.

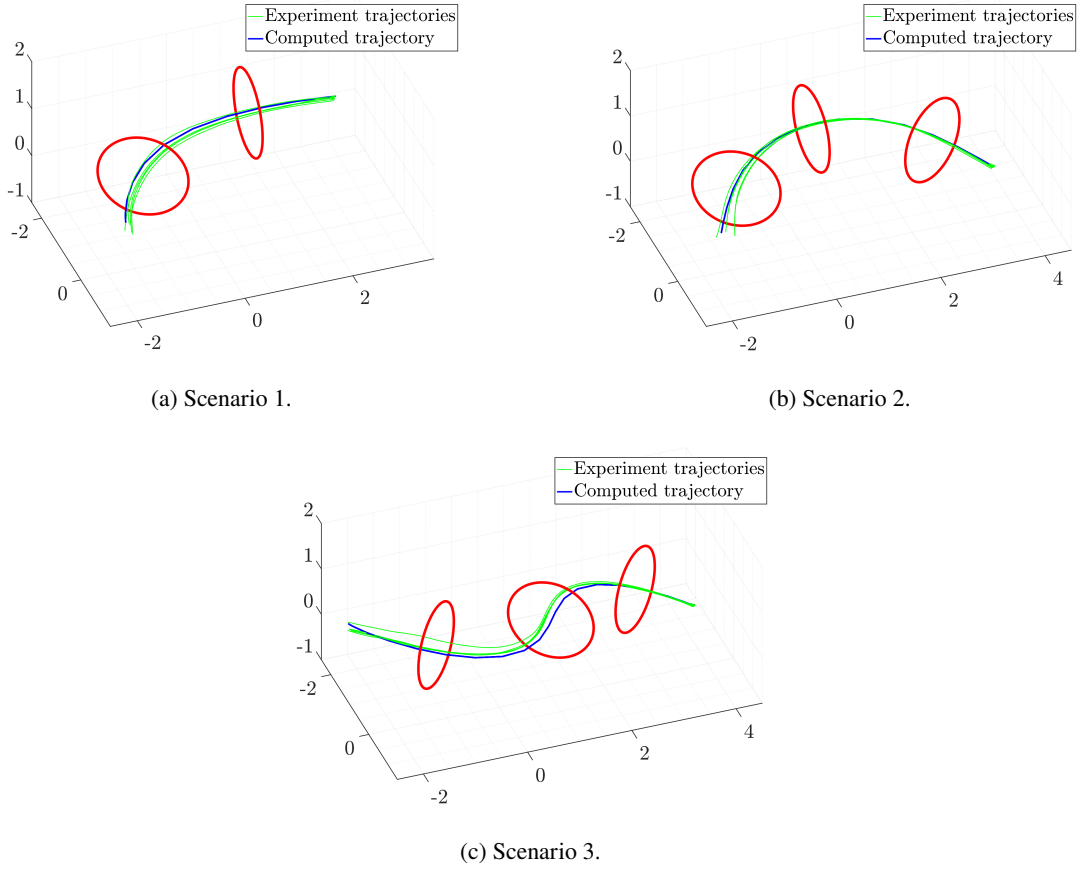


Fig. 10: Reference trajectory computed by Algorithm 1 and Algorithm 2 and the measured flight trajectories in experiments. For each scenario, we showcase the measured trajectories in five separate flight experiments.

- [2] Lan, M., Lai, S., Lee, T. H., and Chen, B. M., “A Survey of Motion and Task Planning Techniques for Unmanned Multicopter Systems,” *Unmanned Syst.*, Vol. 9, No. 02, 2021, pp. 165–198.
- [3] Ioan, D., Olaru, S., Prodan, I., Stoican, F., and Niculescu, S.-I., “From obstacle-based space partitioning to corridors and path planning. a convex lifting approach,” *IEEE Control Syst. Lett.*, Vol. 4, No. 1, 2019, pp. 79–84.
- [4] Ioan, D., Prodan, I., Olaru, S., Stoican, F., and Niculescu, S.-I., “Navigation in cluttered environments with feasibility guarantees,” *IFAC-PapersOnLine*, Vol. 53, No. 2, 2020, pp. 5487–5492.
- [5] Grossmann, I. E., “Review of nonlinear mixed-integer and disjunctive programming techniques,” *Optim. Eng.*, Vol. 3, No. 3, 2002, pp. 227–252.
- [6] Richards, A., and How, J., “Mixed-integer programming for control,” *Proc. Amer. Control Conf.*, IEEE, 2005, pp. 2676–2683.
- [7] Ioan, D., Prodan, I., Olaru, S., Stoican, F., and Niculescu, S.-I., “Mixed-integer programming in motion planning,” *Annu. Rev. Control*, 2020.

- [8] Richards, A., and How, J. P., "Aircraft trajectory planning with collision avoidance using mixed integer linear programming," *Proc. Amer. Control Conf.*, Vol. 3, IEEE, 2002, pp. 1936–1941.
- [9] Mellinger, D., Kushleyev, A., and Kumar, V., "Mixed-integer quadratic program trajectory generation for heterogeneous quadrotor teams," *Proc. IEEE Int. Conf. Robot. Automat.*, IEEE, 2012, pp. 477–483.
- [10] Tang, S., and Kumar, V., "Mixed integer quadratic program trajectory generation for a quadrotor with a cable-suspended payload," *Proc. IEEE Int. Conf. Robot. Automat.*, IEEE, 2015, pp. 2216–2222.
- [11] Landry, B., Deits, R., Florence, P. R., and Tedrake, R., "Aggressive quadrotor flight through cluttered environments using mixed integer programming," *Proc. IEEE Int. Conf. Robot. Automat.*, IEEE, 2016, pp. 1469–1475.
- [12] Gurobi Optimization, LLC, "Gurobi Optimizer Reference Manual," , 2022. URL <https://www.gurobi.com>.
- [13] Mao, Y., Szmuk, M., Xu, X., and Açikmese, B., "Successive convexification: A superlinearly convergent algorithm for non-convex optimal control problems," *arXiv preprint arXiv:1804.06539 [math.OC]*, 2018.
- [14] Szmuk, M., Malyuta, D., Reynolds, T. P., Mceowen, M. S., and Açikmeşe, B., "Real-time quad-rotor path planning using convex optimization and compound state-triggered constraints," *2019 IEEE/RSJ Int. Conf. Intell. Robots Syst.*, IEEE, 2019, pp. 7666–7673.
- [15] Malyuta, D., Reynolds, T. P., Szmuk, M., Lew, T., Bonalli, R., Pavone, M., and Acikmese, B., "Convex optimization for trajectory generation," *arXiv preprint arXiv:2106.09125 [math.OC]*, 2021.
- [16] Mellinger, D., and Kumar, V., "Minimum snap trajectory generation and control for quadrotors," *2011 IEEE Int. Conf. Robot. Automat.*, IEEE, 2011, pp. 2520–2525.
- [17] Yu, H., Wang, Y., Bortoff, S. A., and Ueda, K., "Energy-efficient trajectory planning for a mobile agent by using a two-stage decomposition approach," *IFAC Proceedings Volumes*, Vol. 47, No. 3, 2014, pp. 3851–3856.
- [18] Deits, R., and Tedrake, R., "Efficient mixed-integer planning for UAVs in cluttered environments," *2015 IEEE international conference on robotics and automation (ICRA)*, IEEE, 2015, pp. 42–49.
- [19] Watterson, M., and Kumar, V., "Safe receding horizon control for aggressive MAV flight with limited range sensing," *2015 IEEE/RSJ Int. Conf. Intell. Robots Syst.*, IEEE, 2015, pp. 3235–3240.
- [20] Liu, S., Watterson, M., Tang, S., and Kumar, V., "High speed navigation for quadrotors with limited onboard sensing," *2016 IEEE Int. Conf. Robot. Automat.*, IEEE, 2016, pp. 1484–1491.
- [21] Janeček, F., Klaučo, M., Kalúz, M., and Kvasnica, M., "OPTIPLAN: A MATLAB toolbox for model predictive control with obstacle avoidance," *IFAC-PapersOnLine*, Vol. 50, No. 1, 2017, pp. 531–536.
- [22] Liu, S., Watterson, M., Mohta, K., Sun, K., Bhattacharya, S., Taylor, C. J., and Kumar, V., "Planning dynamically feasible trajectories for quadrotors using safe flight corridors in 3-d complex environments," *IEEE Robot. Automat. Lett.*, Vol. 2, No. 3, 2017, pp. 1688–1695.

- [23] Mohta, K., Watterson, M., Mulgaonkar, Y., Liu, S., Qu, C., Makineni, A., Saulnier, K., Sun, K., Zhu, A., Delmerico, J., et al., “Fast, autonomous flight in GPS-denied and cluttered environments,” *Journal of Field Robotics*, Vol. 35, No. 1, 2018, pp. 101–120.
- [24] Gao, F., Wu, W., Pan, J., Zhou, B., and Shen, S., “Optimal time allocation for quadrotor trajectory generation,” *2018 IEEE/RSJ Int. Conf. Intell. Robots Syst.*, IEEE, 2018, pp. 4715–4722.
- [25] Szmuk, M., Pascucci, C. A., Dueri, D., and Açikmeşe, B., “Convexification and real-time on-board optimization for agile quad-rotor maneuvering and obstacle avoidance,” *2017 IEEE/RSJ Int. Conf. Intell. Robots Syst.*, IEEE, 2017, pp. 4862–4868.
- [26] Szmuk, M., Pascucci, C. A., and Açikmeşe, B., “Real-time quad-rotor path planning for mobile obstacle avoidance using convex optimization,” *2018 IEEE/RSJ Int. Conf. Intell. Robots Syst.*, IEEE, 2018, pp. 1–9.
- [27] Yu, Y., Elango, P., and Açikmeşe, B., “Proportional-Integral Projected Gradient Method for Model Predictive Control,” *IEEE Control Syst. Lett.*, 2020.
- [28] Yu, Y., Elango, P., Topcu, U., and Açikmeşe, B., “Proportional–integral projected gradient method for conic optimization,” *Automatica*, Vol. 142, 2022, p. 110359.
- [29] Yu, Y., and Topcu, U., “Proportional-Integral Projected Gradient Method for Infeasibility Detection in Conic Optimization,” *arXiv preprint arXiv:2109.02756 [math.OC]*, 2021.
- [30] Yu, Y., Elango, P., Açikmeşe, B., and Topcu, U., “Extrapolated Proportional-Integral Projected Gradient Method for Conic Optimization,” *arXiv preprint arXiv:2203.04188 [math.OC]*, 2022.
- [31] Yu, Y., Açikmeşe, B., and Mesbahi, M., “Mass–spring–damper networks for distributed optimization in non-Euclidean spaces,” *Automatica*, Vol. 112, 2020, p. 108703.
- [32] Yu, Y., and Açikmeşe, B., “RLC Circuits-Based Distributed Mirror Descent Method,” *IEEE Control Syst. Lett.*, Vol. 4, No. 3, 2020, pp. 548–553.
- [33] Kuczyński, J., and Woźniakowski, H., “Estimating the largest eigenvalue by the power and Lanczos algorithms with a random start,” *SIAM J Matrix Anal. Appl.*, Vol. 13, No. 4, 1992, pp. 1094–1122.
- [34] Bauschke, H. H., and Combettes, P. L., *Convex analysis and monotone operator theory in Hilbert spaces*, Vol. 408, Springer, 2017.
- [35] Bauschke, H. H., Bui, M. N., and Wang, X., “Projecting onto the intersection of a cone and a sphere,” *SIAM J. Optim.*, Vol. 28, No. 3, 2018, pp. 2158–2188.
- [36] Lofberg, J., “YALMIP: A toolbox for modeling and optimization in MATLAB,” *Proc. IEEE Int. Conf. Robot. Automat.*, IEEE, 2004, pp. 284–289.

- [37] Domahidi, A., Chu, E., and Boyd, S., “ECOS: An SOCP solver for embedded systems,” *Proc. Eur. Control Conf.*, IEEE, 2013, pp. 3071–3076.
- [38] Malyuta, D., Yu, Y., Elango, P., and Açıkmeşe, B., “Advances in trajectory optimization for space vehicle control,” *Annual Reviews in Control*, 2021.